Turkish Journal of Electrical Engineering & Computer Sciences

http://journals.tubitak.gov.tr/elektrik/

Research Article

Turk J Elec Eng & Comp Sci
(2018) 26: 2846 – 2857
© TÜBİTAK
doi:10.3906/elk-1711-243

Reconstruction of geometrical and reflection properties of surfaces by using structured light imaging technique

Şükrü OZAN[1,*], Şevket GÜMÜŞTEKİN[2]
[1]AdresGezgini Inc. Research and Development Center, İzmir, Turkey
[2]Department of Electrical & Electronics Engineering, Faculty of Engineering, İzmir Institute of Technology, Urla, İzmir, Turkey

Received: 20.11.2017 • **Accepted/Published Online:** 06.07.2018 • **Final Version:** 29.11.2018

Abstract: When a robust and dense surface reconstruction is aimed, structured light imaging techniques are usually much appreciated. In this paper we propose a method to reconstruct both geometrical and reflective properties of surfaces by using structured light imaging. We use a technique where a camera and a projector are both treated as viewing devices. They are calibrated in the same manner. Each visible point can be correctly located on both image planes without solving a correspondence problem; hence, a dense reconstruction can be obtained. Since both the camera and the projector are explicitly calibrated, lighting and viewing directions can be identified for each surface point. It is also possible to measure reflected radiance by using high dynamic range (HDR) images for each surface point. The lighting and viewing directions that are known after calibration are combined with the reflected radiance and the incoming irradiance measurements to determine the bidirectional reflectance distribution function (BRDF) values of the material at the reconstructed surface points. We illustrate the reconstruction of surface reflection properties of sample surfaces by fitting the Phong BRDF model to the BRDF measurements.

Key words: Surface reconstruction, structured light, BRDF, surface reflection, HDRI

1. Introduction

Dense surface reconstruction is one of the great challenges in computer vision. Multiview imaging is the most common method to obtain scene depth information. The stereo matching problem (SMP) is at the core of these methods, which has to be solved robustly. Common algorithms to solve the SMP and their performance comparisons can be found in [1].

For surfaces with insufficient textural features, the SMP cannot be robustly solved; hence, an accurate dense surface reconstruction is not possible using stereo imaging. 3D object scanners, which use laser stripes (e.g., [2]) can overcome this problem. These systems make it possible to obtain a dense surface reconstruction even for object surfaces without textural features.

Like laser scanning systems, projector-based structured light systems are also capable of capturing surface geometry robustly. In this work we focus on projector-based 3D reconstruction. We show that these systems can yield not only a dense reconstruction of surface geometry but also measurement of surface reflection properties.

We start by calibrating a projector and a camera as in [3]. Using the fact that the projector has a front end similar to a vision camera, we can calibrate the projector like a camera. The calibrated system can be considered as a stereo imaging system.

*Correspondence: sukruozan@adresgezgini.com

This work is licensed under a Creative Commons Attribution 4.0 International License.

The main aim of this study is to extract reflection properties of the surfaces while making measurements for surface reconstruction. Since both the projector and the camera are explicitly calibrated, for every point on the surface, incoming light and viewing directions can be found if the surface normal directions are calculated correctly. Once the surface irradiance and radiance in the viewing direction is found for each point, a BRDF measurement dataset, which is a subset of the full BRDF, can be generated.

2. Related work

Analysis and comparison of structured light surface reconstruction systems can be found in [4]. If the aim is to simply model surface geometry, even a single image can be sufficient when color-coded stripe patterns are used [5], but color-coded stripes are not easy to decode when the object chromaticity is not homogeneous on the surface. In [6] a more complex system with two projectors and one camera, which is capable of making reconstructions by a single shot, was proposed to overcome this problem.

Binary coded patterns are much easier to decode since they are not severely affected by surface chromaticity. However, it is hard to differentiate ON - OFF states of a projector pixel for binary coded patterns representing least significant bits of pixel position. Binary gray coded patterns make it possible to overcome this problem since in this coding system two successive values differ in only one bit. This allows the thin stripes to be thicker and more distinguishable. We follow the robust pixel classification algorithm given in [7] where gray coded patterns are used. This method inherits the direct and global illumination component separation method proposed in [8]. Once the scene is illuminated by the successive binary gray coded patterns, robust pixel classification can be used to find ON-OFF pixels and hence projector pixel locations can be decoded.

Accurate calibration of both the projector and the camera is a prerequisite for the overall procedure. We used Zhang's homography approach for camera calibration [9]. We adapted the local homography approach reported in [10] to calibrate the projector.

In this work we show that projector-based surface reconstruction can also be used to capture physical properties of surfaces under some assumptions and conditions. The most convenient way of representing surface reflection properties is to use BRDFs. Since BRDF is the ratio of reflected radiance to incident irradiance, we need to have the corresponding radiance and irradiance measurements. By using the methodology in [12] we can estimate the camera response function for each of three-color channels, red, green, and blue (RGB). The response function estimation makes it possible to find absolute radiance values at surface points.

Surface normal directions, surface lighting, and viewing directions together with the radiance measurements constitute a dataset, which is a subset of the BRDF that defines a material's interaction with the light. In the literature, there are complex BRDF measurement systems capable of measuring BRDF almost completely, such as in [13]. In this study our main contribution is to show that the proposed 3D scanning system can also generate partial BRDF data, which later can be used to approximately reconstruct surface reflectance properties of surfaces by fitting an analytical BRDF model.

There are several analytical BRDF models in the computer graphics literature. These models have the ability of capturing reflection properties of materials and they are widely used in ray tracing software. Moreover, these models are fitted to dense BRDF measurements, such as Matusik's database [13], which is the most comprehensive open BRDF measurement database, and they are used to simulate corresponding materials reflection properties in ray tracing software.

Some analytical BRDF models are also capable of capturing complex reflection features such as anisotropy [14,15]. In this study the measured BRDF data are limited to the specular plane of incidence. We assume that

the materials under consideration have isotropic reflection properties. We use the Phong model for data fitting. Despite its low complexity, the Phong model makes it possible to approximate the specular lobe around the measured data in the direction of specular reflection.

These related works propose a novelty either in reconstructing surface geometry or measuring surface reflectance properties. On the contrary, this study does not aim to propose a novelty in either of the areas. Instead, it aims to simultaneously reconstruct geometry and reflection properties of surfaces having arbitrary geometry by using state of the art methods in surface reconstruction together with HDR imaging techniques.

This novel approach, which was thoroughly explained in the corresponding PhD thesis [16], makes it possible to use a camera-projector scanning system to be used not only for reconstructing the surface geometry but also surface reflection properties.

3. Calibration of system components

Since accurate 3D data acquisition from the scene is a crucially important part of the overall procedure, the system components, the camera and projector, should be precisely calibrated.

3.1. Camera calibration

Zhang's method [9] is a convenient way to estimate camera calibration parameters from 2D views of a calibration pattern. In this work we use a 20 ×14 checkerboard pattern. The method uses homography correspondence between the world coordinates and image coordinates of feature points on the pattern. The radial lens distortion is an important artifact that should be handled. The method in [9] makes it possible to embed the distortion parameters (k_1, k_2) into the system and can estimate them together with the intrinsic and extrinsic camera parameters. The lens distortion can be modeled as in Eq. (1).

$$\begin{aligned} u &= u_d + (u_d - u_0)\left[k_1\left(x^2 + y^2\right) + k_2\left(x^2 + y^2\right)^2\right], \\ v &= v_d + (v_d - v_0)\left[k_1\left(x^2 + y^2\right) + k_2\left(x^2 + y^2\right)^2\right] \end{aligned} \tag{1}$$

$(u,\ v)$ are the ideal (undistorted) pixel coordinates where $(u_d\ ,\ v_d)$ are the observed (distorted) pixel coordinates. (x, y) represent ideal image coordinates. System parameters, including distortion parameters, are estimated in an optimization procedure (a MATLAB implementation of the Levenberg–Marquardt nonlinear regression method).

3.2. Projector calibration

In [3] it was suggested that we can model the projector as a capturing device. Once we find the projection of the feature points on the CCD of the projector, we can calibrate the projector just like a camera.

The projector we use in this work is an HD projector (i.e. 1920 ×1080 resolution). We used the same calibration pattern used in camera calibration. The only difference is that we project 22 column and row encoding stripe patterns (11 for column encoding, see Figure 1a, and 11 for row encoding, see Figure 1b). The calibration pattern is illuminated by consecutive structured light patterns. Before calibrating the projector two major steps should be performed. First, scene images illuminated by structured light patterns should be decoded. Second, the projected feature points on the projector CCD array should be identified. By following these steps we could accurately calibrate the camera-projector pair.

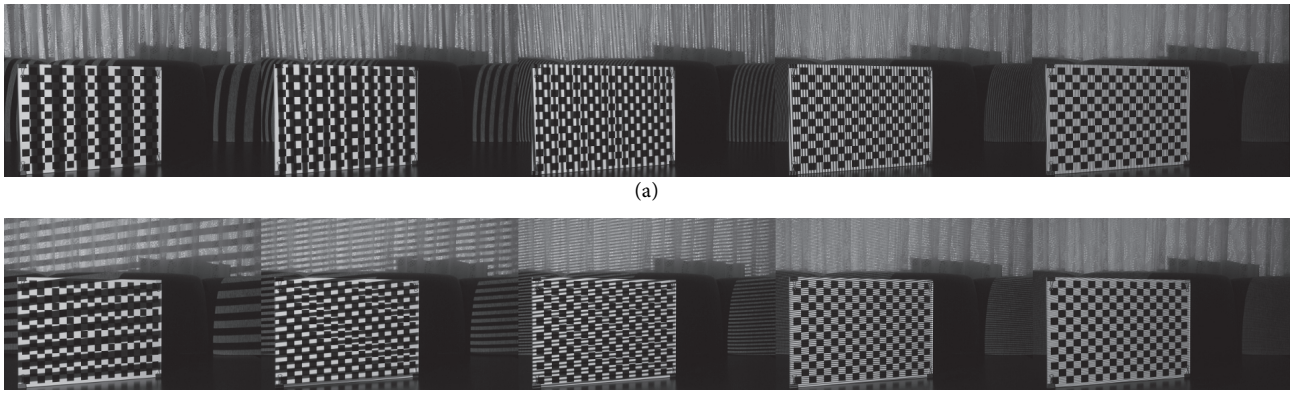

(a)

(b)

Figure 1. Scene illuminated by (a) column encoded and (b) row encoded light patterns. Least significant five patterns can be seen for each case.

3.3. Robust pixel classification

Decoding light patterns is not a straightforward task and should be handled carefully. The idea is to find the ON-OFF state of the corresponding projector pixels in each captured image. Simple thresholding does not work at a desired level of precision to detect the pixel state. Robust pixel classification [7] uses an enhanced thresholding algorithm, which is based on the method of separating direct and global components of a reflection [8].

3.4. Finding feature points at the projector side

We first find the subpixel coordinates of the feature points of the calibration pattern in the images captured by the camera using back projection as illustrated in Figure 2. This information is used to calibrate the camera.

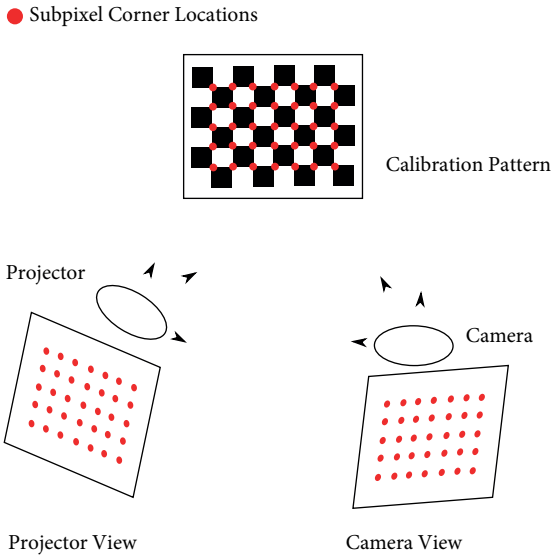

Figure 2. Subpixel corner locations found on the image are taken by camera, then these pixel positions are projected back to the projector image plane. Local homography method is used for projection [10].

We only calculate the values in a window around detected checkerboard corners locally to reduce processing time. The size of the window may vary with respect to the image size. In this work we use 30 px by 30 px windows to decode projector pixel coordinates. Locally decoded pixel values are used to find the projection of feature points, detected on the captured images, at the projector side. As a result we can find subpixel positions of feature points in the projectors virtual view for 5 different calibration pattern positions. By applying the same procedures explained for camera calibration, we can also calibrate the projector with subpixel accuracy.

4. Reconstruction of surface geometry

Without solving an SMP, we can directly calculate the subpixel positions on both the camera and projector image plane for any point, if it is visible by camera and illuminated by the projector. Since we have two corresponding pixel positions in two different views, the depth finding problem can be solved by solving a singular value decomposition (SVD) problem for each surface point. In order to eliminate redundant areas and to speed up the process, we select region of interest (ROI) over the scene image using a graphical interface in MATLAB. In Figure 3, three of our sample scenes that include objects with different types of materials and corresponding reconstructions can be seen. The system is capable of generating a very dense point cloud of an object once the object is visible both by camera and projector.

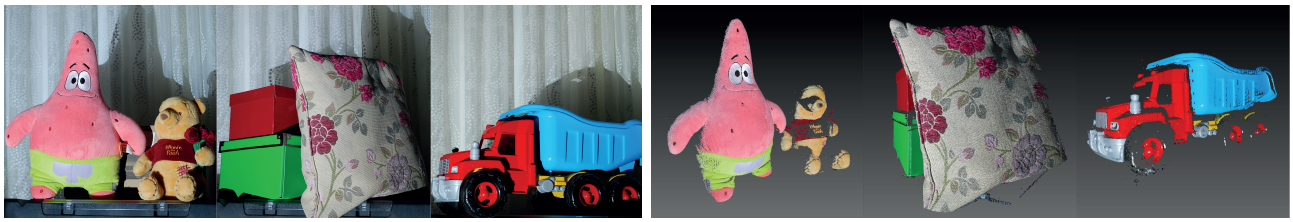

(a) (b)

Figure 3. (a) Three experiments performed using different objects with various surface characteristics. (b) Dense point clouds of objects in (a).

The objects are selected to show how the proposed system is capable of reconstructing surfaces of different kinds of objects and materials (see Figure 3a). Figure 3b is the reconstructed dense point clouds of the corresponding objects given in Figure 3a viewed from slightly changed viewing directions (with respect to the camera view in Figure 3a).

5. Reconstruction of surface reflection properties

In this work we aim to use the proposed scanning system such that it can also measure a significant part of the BRDF. Hence, we need lighting and viewing directions along with irradiance and radiance measurements for reconstructed surface points.

5.1. Estimation of surface normals in a point cloud data

The scanner system described above is able to generate dense point cloud data of scanned objects. The generated point clouds closely approximate the surface geometry of the scanned objects. We use the surface normal estimation technique in [17], which is a robust method for estimating surface normals in noisy point cloud data.

Surface normals at each point in the point cloud can be found by locally applying the total least square line method. The surface normals are calculated in a small neighborhood of each point in the cloud. The

selection of neighborhood size is important and it affects the normal estimation. As in [17] we empirically estimate the neighborhood (r) size. If it is too small, the estimated normal directions are distorted. The importance of neighborhood size selection can be seen in Figure 4. In Figure 4a, r is chosen so small that the estimated normal directions are not properly aligned. In Figure 4b, r is selected appropriately and estimated normal direction vectors are correctly aligned.

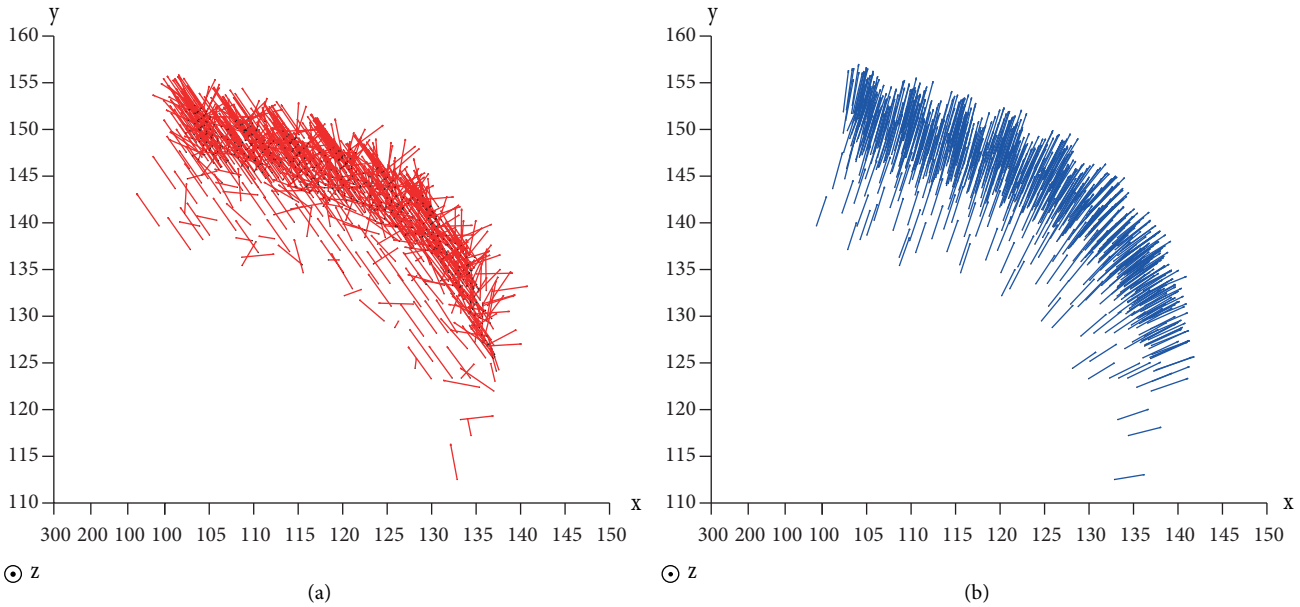

Figure 4. The selection of neighborhood size r is important. (a) r is too small, normal directions are distorted. (b) r is properly selected, directions are aligned correctly.

We use this information to identify the BRDF of a given surface since BRDF is defined by incoming and outgoing light directions, which should be defined with respect to the surface normal.

5.2. Measuring radiance by using high dynamic range imaging

A camera captures radiance reflected from a scene. Every capturing device, either digital or analog, can be represented by a response function, which identifies the device's behavior to the amount of irradiance incident to its sensor. The camera response function relates image irradiance at the image plane to measured pixel intensity values. It is possible to find a camera response function by capturing a calibration target at various exposure levels. We have implemented the method used in [12] to find our camera's response functions for three color channels. An image radiance map can be calculated by using these response functions.

The recovered camera response function for the green channel can be seen in Figure 5a. As stated in [12], theoretically, at least two images taken using two distant exposures are enough to recover the film response curve. In the above analysis, we used images captured with different exposure intervals from 1/40,000 to 30 s. We also analyzed the effect of the number of images used in radiance calculations. In Figure 5b, reconstructed exposure and log exposure values of 1000 randomly selected pixels for 18, 9, 5, and 3 images can be seen. If we consider recovered radiance values, which are calculated by using 18 images as a ground truth, we can see that radiance values calculated by using 9 and 5 images are nearly the same as the ground truth values, but if 3 images are used the result deviates from the ideal values. Hence, for most practical cases 5 images with 5

distant exposure values can be efficiently used to model the camera's response function and to recover desired scene radiance values.

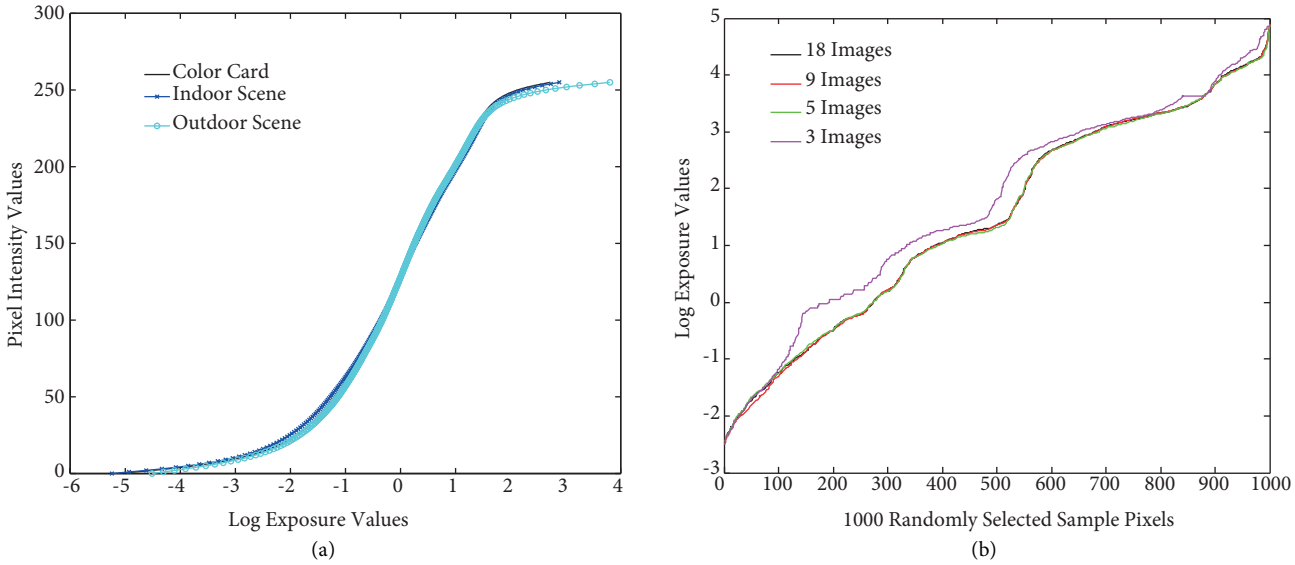

Figure 5. (a) Green channel component of the response function of Nikon D60 recovered by using log radiance values for 1000 randomly selected samples from the scene. (b) The radiance plots generated by using 18, 9, 5, and 3 images.

5.3. Estimation of surface radiance

To measure the BRDF of a material, we need to have the radiance data in the direction of the viewer. We compute the required scene radiance map by using the HDRI technique reported in [12]. The known radiance value of a luminaire is used to scale the camera response function and once the camera response function is scaled it can be used to find absolute radiance values. In our implementation we used the illumination specs of the projector to find the corresponding scale factor.

5.4. Estimation of surface irradiance

The surface irradiances of the objects used in the experiments are directly related to the projector power and the projection area. By using the projector's luminous flux and the distance of infinitesimal surface area to the projector, the corresponding surface irradiance can be calculated. It is important to consider the foreshortening, which is known from the surface normal and the illumination directions (i.e. $(\omega_i \cdot \mathbf{n})$).

5.5. Generating BRDF measurement dataset

One of our main assumptions is that the reflections have isotropic nature, i.e. the surface reflection properties do not vary if we rotate (ω_i, ω_o) pair around the surface normal **n,** where ω_i and ω_o represent incoming and outgoing light directions with respect to the surface normal **n**. Some materials such as velvet do exhibit anisotropic reflection characteristics. Measuring anisotropic reflection is a much more complicated process. In [14] a typical setup is proposed to measure anisotropic BRDFs.

Since we assume isotropy we do not consider objects made of anisotropic materials like the teddies in Figure 3a. Instead, we consider plastic and rough metal surfaces given in Figures 6a and 6b and assume isotropy for these materials.

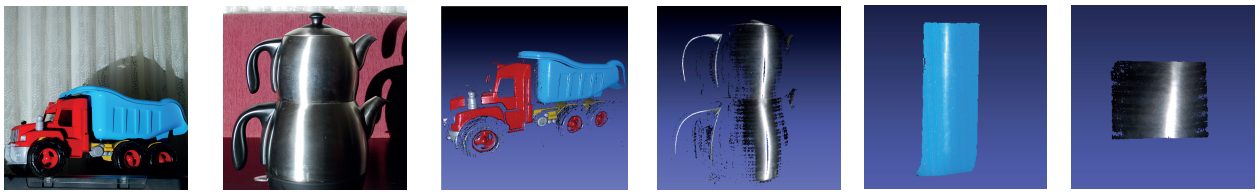

(a) (b) (c) (d) (e) (f)

Figure 6. (a, b) Two experimental scenes in which a plastic toy truck and a rough steel teapot can be seen. (c, d) Corresponding reconstructions of the objects. (e, f) Sample areas selected over the reconstruction results. These areas have both specular and diffuse reflection characteristics.

Reconstructed 3D point clouds of objects in Figures 6a and 6b are shown in Figures 6c and 6d. In order to reconstruct the surface reflection properties of these objects, we select sample areas shown in Figures 6e and 6f, on the surfaces where both specular and diffuse reflection can be observed. We use radiance measurements at the points on these sample surface patches to identify the reflection properties of corresponding materials.

The calibrated system together with surface normal gives us $(\omega_i\,,\ \omega_o)$ pairs for each surface point on the selected sample surfaces. Using the precomputed irradiance (E) and radiance (L), we can calculate the BRDF (f_r) at a surface point as in Eq. (2).

$$f_r\left(\omega_i, \omega_o\right) = \frac{dL_r(\omega_o)}{dE_i(\omega_i)} = \frac{dL_r(\omega_o)}{L_i\left(\omega_i\right)\left(\omega_i \cdot \mathbf{n}\right) d\omega_i} \tag{2}$$

The direction vectors $\mathbf{n}$, ω_i, and ω_o can be represented by unit vectors in spherical coordinates with respect to the surface normal for each sample surface point. A unit vector is represented by two angles, elevation θ and azimuth φ, in the spherical coordinate system. Since the materials are assumed to be isotropic, incoming and outgoing vectors can be represented with three angles, θ_i, θ_o, and $\varphi\,(i.e.\ \varphi = |\varphi i - \varphi o|)$. The isotropic BRDF measurements can be tabulated by using these three angles and BRDF values for three color channels. In Table 1, some of our BRDF measurement data for rough metal surface can be seen. The first three columns are angle values, which define an isotropic BRDF. The remaining three columns are values of the BRDF for red, green, and blue channels, respectively. The conventions of computer graphics literature were used while creating this table.

Table 1. Tabulated sample BRDF measurements of the rough steel material in Figure 6f.

$\theta_\mathbf{i}$	$\theta_\mathbf{o}$	ϕ	Red	Green	Blue
24.4471	20.0176	179.3658	4.5079	4.7198	4.4124
24.4471	20.0176	179.3658	4.5079	4.7198	4.4124
24.7140	20.0037	179.2479	3.8747	3.9278	3.8436

The tabulated data of a complete BRDF dataset can be used directly in rendering processes, but the partial data we measure are not sufficient to be used in a rendering process since they do not cover all the incoming and outgoing light direction combinations of a reflection defined on a surface point. In order to be able to use partial measurements in the rendering process, we need to use an analytical BRDF model's fitted measured data. Since we assume that the surfaces have isotropic nature, we choose the Phong BRDF model, which can handle isotropic material reflections. The Phong model is a popular model, which is widely used in computer graphics applications. In this model (Eq. (3)), r is the unit vector in the direction of the specular

reflection, where ω_i shows incoming light direction and $\mathbf{n}$ shows the surface normal direction. ρ_d and ρ_s values are diffuse and specular reflection coefficients, respectively. Figure 7 illustrates how parameter m affects rendered images.

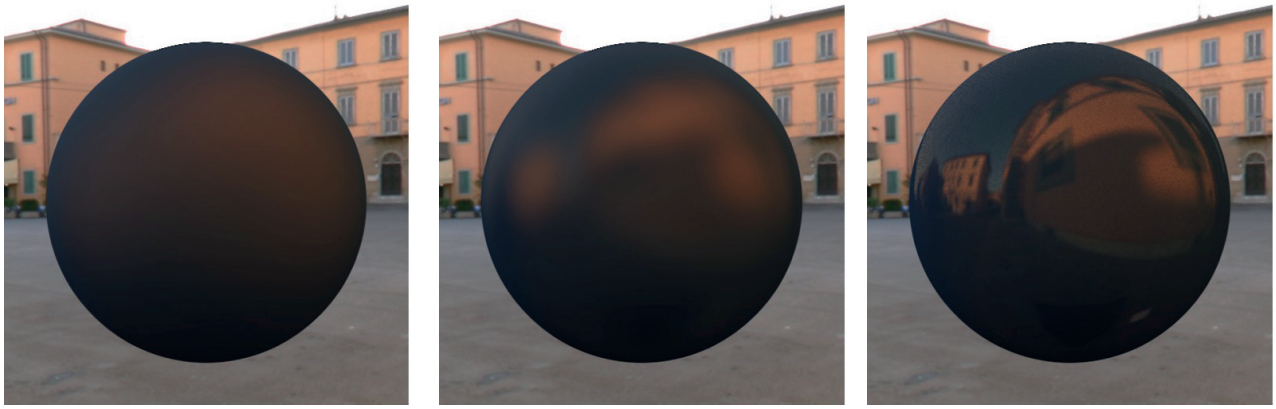

(a) m = 4.0 (b) m = 40.0 (c) m = 4000.0

Figure 7. The Phong BRDF model can capture specularity. Higher lobe exponent m creates more specularity in renders.

$$f(\omega_i, \omega_o) = \frac{\rho_d}{\pi} + \rho_s (\omega_o \cdot \mathbf{r})^m \quad where\, \mathbf{r}{=}2(\omega_i \cdot \mathbf{n})\mathbf{n} - \omega_i \tag{3}$$

As proposed in [14] and [15], the parameters of an analytical BRDF model can be found by minimizing the error function $E(\boldsymbol{p})$ given in Eq. (4). $R(\omega_i, \omega_o)$ represents the measured BRDF value at given incoming and outgoing light directions and $M(\omega_i, \omega_o; \mathbf{p})$ represents the model BRDF value with the model parameters represented by vector $\mathbf{p}$.

$$E(\mathbf{p}) = \sqrt{\frac{\sum w \left[R(\omega_i, \omega_o)\cos\theta_i - M(\omega_i, \omega_o; \mathbf{p})\cos\theta_i\right]^2}{\sum w}} \tag{4}$$

In order to model reflection properties of a material we have to model both the diffuse and specular reflection. The sample surface patches we selected over the reconstructed material surfaces have sufficient information to model diffuse reflection since the amount of off-specular reflection samples is much more than samples around the direction of specular reflection. If we consider r vector, which represents the direction of specular reflection, we choose weight parameters w to be equal to $(\omega o \cdot \mathbf{r})$. This choice of w can handle the specular lobe well for our limited BRDF measurements, which are mostly distributed around the specular reflection direction.

6. Results and conclusions

6.1. Results

Estimated Phong model parameters for the two sample materials are given in Table 2. The model parameter m, which defines the specular lobe of reflection, is as expected a high value since both materials have an obvious specular reflection feature. The blue channel diffuse component of blue plastic is estimated as much higher than the red and green components, which by intuition is also an expected result.

In Figure 8, we show the measured data (blue dots) and fitted analytical model values (red curve). The vertical axis represents the BRDF value and the horizontal axis represents the angle between ω_o and r. The

Table 2. Estimated Phong model parameters for two sample materials. $\rho_d^{\mathbf{C}}$ represents diffuse component for color channel C (R, G, or B). m is the parameter that defines specular lobe. Higher m means more specularity.

Material	$\rho_{\mathbf{d}}^{\mathbf{R}}$	$\rho_{\mathbf{d}}^{\mathbf{G}}$	$\rho_{\mathbf{d}}^{\mathbf{B}}$	$\rho_{\mathbf{s}}^{\mathbf{R}}$	$\rho_{\mathbf{s}}^{\mathbf{G}}$	$\rho_{\mathbf{s}}^{\mathbf{B}}$	$\mathbf{m}$
Blue plastic	0.1040	0.7825	2.0697	0.0293	0.0465	0.0612	1.1512e+02
Rough steel	0.1052	0.1230	0.1316	0.2815	0.2871	0.2849	1.1760e+02

increase in BRDF values near the specular reflection direction (i.e. as the angle between ω_o and r gets smaller) can be seen. In order to visualize the measured reflection properties of the sample materials, the Phong model is used in a ray tracer software called Physically Based Rendering Toolkit (PBRT) [18] with estimated model parameters.

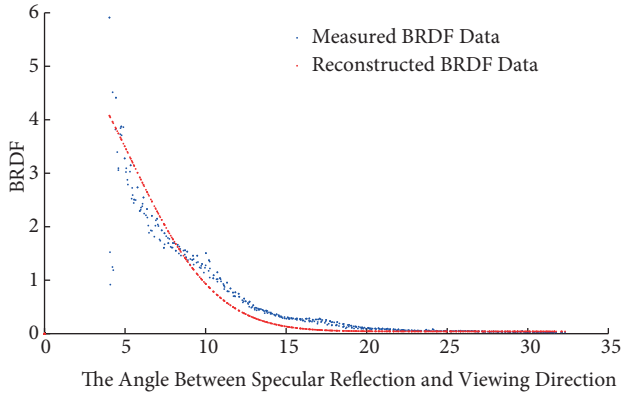

Figure 8. Measured and corresponding fitted Phong BRDF samples shown for rough steel material.

In Figure 9, we show synthetic scenes by using the Phong BRDF model for 2 different parameter sets estimated for 2 different materials, namely blue plastic and rough steel. One object is a simple ball, seen in Figures 9a and 9b, and the other is the well-known Buddha model, seen in Figures 9c and 9d. Our aim is to show that an analytical BRDF model with estimated parameters gives the desired feeling for the corresponding materials in rendered scenes.

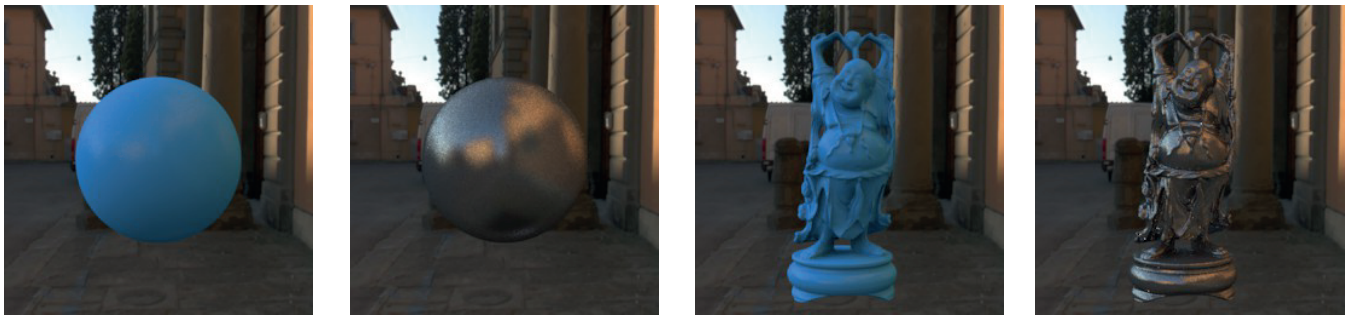

(a) (b) (c) (d)

Figure 9. Synthetically rendered scenes with estimated Phong model parameters in Table 2. In (a) and (b) estimated Phong model parameters are used to render a ball shape. In (c) and (d) estimated Phong model parameters are used to render a Buddha figure.

7. Conclusions

In this study we propose a method to reconstruct both geometrical and reflective properties of surfaces by using structured light imaging techniques together with HDR imaging techniques. This method relies on the calibration of the intrinsic and extrinsic parameters of the camera and the projector. Corresponding pixel coordinates of the projector and the camera are used to reconstruct the surface geometry in 3D. The same system is also used to measure the scene radiance by using HDRI techniques. Since both the camera and the projector are geometrically calibrated we can calculate incoming and outgoing light directions for each surface point. Hence, the system can also measure BRDF values at reconstructed surface points.

Our BRDF measurements can be used for fitting analytical BRDF models. In this study we used the Phong model and estimated its parameters for different materials. We tested the estimated model parameters on rendered scenes (see Figure 9). It should be noted that in this implementation we are assuming the surface reflections to be isotropic and the selected surfaces to have visible specular highlights, which is necessary to model the specular part of the BRDF.

Methods in reflection measurement literature use complex setups designed to measure surface reflection from every possible lighting and viewing direction. Typically, only geometrically simple objects (e.g., sphere, cylinder) are used. In this study, instead of attempting to measure the BRDF of a material covering an object with simple geometry, we focused on the reconstruction of complex object surfaces, thereby making the information acquired by the camera/projector-based scanning system meaningful for BRDF measurements.

In the 3D reconstruction literature we see that structured light techniques are widely used. These studies usually concentrate on the robustness of proposed systems. Here we add a novel feature to a structured light-based scanning system by using it also for radiance measurements. This study does not aim to propose a novelty either in reconstructing surface geometry or measuring surface reflectance properties, but it certainly does in reconstructing surface geometry and reflection properties simultaneously, because it suggests an idea that proposes to use a camera/projector-based scanning system to be used also as an HDR imaging device, which makes it possible to measure BRDF from geometrically complex object surfaces. The proposed work is a part of a PhD thesis [16], which can be referred to for more details about the used methods and algorithms by interested readers.

References

[1] Tippetts B, Lee DJ, Lillywhite K. Review of stereo vision algorithms and their suitability for resource-limited systems. J Real-Time Image Pr 2016; 11: 5-25.

[2] Ozan Ş, Gümüştekin Ş. Calibration of double stripe 3d laser scanner systems using planarity and orthogonality constraints. Digit Signal Process 2014; 24: 231-243.

[3] Zhang S, Huang PS. Novel method for structured light system calibration. Opt Eng 2006; 45: 1-8.

[4] Geng J. Structured-light 3D surface imaging: a tutorial. Adv Opt Photonics 2011; 3: 128-160.

[5] Wang ZZ, Yang YM. Single-shot three-dimensional reconstruction based on structured light line pattern. Opt Laser Eng 2018; 106: 10-16.

[6] Vo M, Narasimhan SG, Sheikh Y, Texture illumination separation for single-shot structured light reconstruction. IEEE T Pattern Anal 2016; 38: 390-404.

[7] Xu Y, Aliaga DG. Robust pixel classification for 3d modeling with structured light. In: Proceedings of Graph Interfaces; 2007. New York, NY, USA: ACM. pp. 233-240.

[8] Nayar SK, Krishnan G, Grossberg MD, Raskar R. Fast separation of direct and global components of a scene using high frequency illumination. ACM T Graphic 2006; 25: 935-944.

[9] Zhang Z. A flexible new technique for camera calibration. IEEE T Pattern Anal 2000; 22: 1330-1334.

[10] Moreno D, Taubin G. Simple, accurate, and robust projector-camera calibration. In: 2012 Second International Conference on 3D Imaging, Modeling, Processing, Visualization Transmission; 2012; Zurich, Switzerland. New York, NY, USA: IEEE. pp. 464-471.

[11] Debevec PE, Malik J. Recovering high dynamic range radiance maps from photographs. In: Proceedings of the 24th Annual Conference on Computer Graphics and Interactive Techniques; 2008; New York, NY, USA. pp. 369-378.

[12] Matusik W. A data-driven reflectance model. PhD, Massachusetts Institute of Technology, Cambridge, MA, USA, 2003.

[13] Ngan A, Durand F, Matusik W. Experimental analysis of BRDF models. Proceedings of the Sixteenth Eurographics Conference on Rendering Techniques; 2005; Switzerland. pp. 117-126.

[14] Kurt M, Szirmay-Kalos L, Krivanek J. An anisotropic BRDF model for fitting and Monte Carlo rendering. Comp Graph 2010; 44: 1-15.

[15] Ozan Ş. Joint reconstruction of surface geometry and reflection properties by using image based methods. PhD, İzmir Institute of Technology, İzmir, Turkey, 2015.

[16] Mitra NJ, Nguyen A, Guibas LJ. Estimating surface normals in noisy point cloud data. Int J Comput Geom Ap 2004; 14: 261-276.

[17] Pharr M, Humphreys G. Physically Based Rendering: From Theory to Implementation. 2nd ed. San Francisco, CA, USA: Morgan Kaufmann Publishers Inc., 2010.